INTERNATIONAL JOURNAL FOR NUMERICAL METHODS IN FLUIDS
Int. J. Numer. Meth. Fluids 2002; **40**:1275–1302 (DOI: 10.1002/fld.415)

Analysis of the near-wall behaviour of some self-adaptive subgrid-scale models in finite-differenced simulations of channel flow

P. Sagaut[1,2,*,†], E. Montreuil[2], O. Labbé[2] and C. Cambon[3]

[1]*LMM-UPMC, Boite 162, 4 Place Jussieu, 75252 Paris Cedex 05, France*
[2]*ONERA/DSNA, 29 av. de la Division Leclerc, 92 Châtillon, France*
[3]*ONERA and LMFA/ECL, 36 av. Guy de Collongue, BP 163, 69131 Ecully Cedex, France*

SUMMARY

Self-adaptive subgrid-scale models are proposed and assessed. They are based on the use of the Germano–Lilly dynamic procedure and the use of a selection function. These models, which do not incorporate any information related to the location of the solid walls, are well suited for the simulation of turbulent flows in complex geometries. Their reliability, when used together with a second-order non-dissipative numerical method, is assessed on the plane channel configuration for two values of the Reynolds number ($Re_\tau = 180$ and 395) for two grid resolutions. The selection function approach for deriving self-adaptive subgrid models is found to yield results very similar to those obtained using a dynamic model, without requiring any numerical stabilization procedure. The use of the selection function is shown to be the only one which is able to capture the backscatter process in the buffer layer, while producing a strictly positive subgrid viscosity. This is demonstrated to be linked to the capability of the selection function to permit a decorrelation between the mean strain and the fluctuations of the subgrid stresses. That point is illustrated thanks to the introduction of a new decomposition of the fluctuating strain subgrid dissipation. Copyright © 2002 John Wiley & Sons, Ltd.

KEY WORDS: LES; SGS model; plane channel flow

1. INTRODUCTION

Large-eddy simulation (LES, see Reference [1] for a general review) has already been found to be a reliable tool for the unsteady simulation of turbulent, fully developed, equilibrium flows. For this class of applications, both the subgrid-scale (SGS) model and the numerical scheme are generally optimized, i.e. all the available knowledge about the particular flow dynamics is taken into account when designing the SGS model (e.g. homogeneous directions are used for specific purposes), while very high order accurate numerical methods (e.g. spectral, pseudo-spectral or Padé) are used, which ensure that the numerical error will not mask the physical SGS model.

* Correspondence to: P. Sagaut, LMM-UPMC, Boite 162, 4 Place Jussieu, 75252 Paris Cedex 05, France.
† E-mail: sagaut@lmm.jussieu.fr

Received 25 January 2001
Revised 20 May 2002

But even in the simple case of the plane channel flow, recent studies have demonstrated that the classical representation of the interscale transfer as a net drain of the resolved kinetic energy (i.e. the forward energy cascade) is no longer valid. By splitting the subgrid dissipation ε_{sgs} into the sum of the mean strain dissipation ε_{MS} and the fluctuating strain dissipation ε_{FS}, Härtel *et al.* [2] found that there exists a region, located in the buffer zone of the boundary layer, where the latter becomes negative in the mean. This backscatter was shown by Piomelli *et al.* [3] to be strongly correlated with the presence of sweeps, while the forward scatter is associated with ejections. In that zone, an SGS model should be able to account for the net backscatter effect. It was demonstrated in Härtel and Kleiser [4] that none of the classical subgrid-viscosity models (Smagorinsky, Structure Function, Germano-Lilly dynamic model) is able to account for net backscatter, resulting in a strictly positive fluctuating strain SGS dissipation.

Another point is that the use of LES for industrial flows is still a challenging topic, because most of the advantages present in academic flows, like isotropic turbulence, plane channel flow, time developing mixing layer, etc. are now lost. Such flows involve complex dynamics and complex geometries, and most of the techniques that were designed to recover good results for academic configurations cannot be used anymore. As an example, let us consider that a correct description of the boundary layers is of great importance for such applications (heat transfer, skin friction, fluid–structure interaction), and that the SGS models must allow the simulation to capture correctly its dynamics. Because several solid walls are generally involved, and a multi-domain technique may be used as in Mary and Sagaut [5], the distance to the wall is often difficult to evaluate and then must not be incorporated into the SGS model. Thus, the use of a van Driest-like damping function, as done in Piomelli *et al.* [6], is then to be excluded. The averaging technique along a plane parallel to the wall (i.e. in homogeneous directions), as employed in Schumann's split SGS model [7], has also to be avoided: because when using an automatic mesh generator, the mesh is not constrained to stay at a given distance from the wall expressed in wall units, and non-equilibrium spatially-developing boundary layers should be considered. In these cases, the grid points belonging to the same plane do not constitute a statistical equivalence class, i.e. the probability density function of the velocity component is not identical for all these points. As a consequence, the plane averaging operator is not equivalent to a statistical average, and cannot be employed. The case of unstructured meshes is even more constraining, because the concept of grid plane is no longer valid.

The aim of the present work is to propose and assess SGS models which are (i) able to reproduce correctly the interscale energy transfer between resolved and subgrid scales, including backscatter in the near-wall region and, (ii) suitable for complex geometries, i.e. which involve only a 5-point (in each direction) compact stencil. These models will be referred to as self-adaptive models, because they do not incorporate any information related to the location of the solid walls. They are obtained in the present work using a selection function, as proposed by David [8] for modifying the Structure Function model (see also Métais and Lesieur [9] and Sagaut [1]) for the capture of transition and modified in order to appear as a continuous function by Sagaut and Troff [10]. New self-adaptive versions of two basic subgrid-viscosity models, (Smagorinsky, Mixed Scale Model) are proposed in the present paper, to demonstrate the generality of the proposed self-adaptation procedure. Results will be compared to those obtained using the Germano–Lilly dynamic model based on a fully

three-dimensional test filter and the selective Structure Function model. It is worth noting that almost all the results previously obtained with a dynamic model on the channel flow configuration were based on two-dimensional test filters.

Another important point is that we are interested here in analysing the behaviour of the models in conditions which are close to those of future industrial applications. Thus, mesh size analogous to those used in complex configurations at high Reynolds number are employed, leading to the definition of coarse grids when compared to those found in papers dealing with computations of 'best' possible LES results. In the same spirit, a second-order accurate numerical scheme will be employed.

The selected test case is the incompressible channel flow, because corresponding complete data sets are available. Two Reynolds numbers based on the friction velocity are considered: $Re_\tau = 180$ and 395, corresponding to the direct numerical simulation (DNS) data base of Kim *et al.* [11] and Mansour *et al.* [12]. Two grids are considered, in order to analyse the response of such SGS models for various degrees of resolution.

To get a deeper insight into the response of the SGS models, the SGS dissipation is investigated on the grounds of the double decomposition introduced by Härtel *et al.* [2]. To assess the possibility of reproducing backscatter with strictly positive subgrid-viscosity SGS models, a new triple decomposition of the fluctuating strain SGS decomposition is proposed.

The paper is organized as follows: Section 2 describes the governing equations and the selected SGS models, while Section 3 presents the numerical method. Characteristics of the different simulations are given in Section 4. The results are compared to DNS data and dynamic model results in Section 5, and the SGS models behaviour is analysed in Section 6. Conclusions are given in Section 7.

2. GOVERNING EQUATIONS AND SGS MODELS

2.1. Filtered Navier–Stokes equations

The governing equations for the large-eddy simulation of an incompressible fluid flow are derived by applying a convolution filter to the Navier–Stokes equations. The resulting set of non-dimensional equations reads:

$$\frac{\partial \bar{\underset{\sim}{u}}}{\partial t} + \nabla \cdot (\bar{\underset{\sim}{u}} \otimes \bar{\underset{\sim}{u}}) = -\nabla \bar{p} + \frac{1}{Re} \nabla^2 \bar{\underset{\sim}{u}} - \nabla \cdot \tau \tag{1}$$

$$\nabla \cdot \bar{\underset{\sim}{u}} = 0 \tag{2}$$

where the Reynolds number is calculated using the reference velocity U_0 and the reference lengthscale L_0 of the non-dimensionalization. The subgrid tensor τ is defined as

$$\tau = \bar{\underset{\sim}{u}} \otimes \bar{\underset{\sim}{u}} - \overline{\underset{\sim}{u} \otimes \underset{\sim}{u}} \tag{3}$$

and needs to be parameterized. The SGS models used in the present study will be discussed in the next section. Because only eddy-viscosity type models are considered, the isotropic part of the SGS tensor is added to the filtered pressure, leading to the definition of a pseudo-pressure referred to as Π:

$$\Pi = \bar{p} + \tfrac{1}{3}\tau_{kk} \tag{4}$$

where

$$\tau_{kk} = \mathrm{Tr}(\tau) \tag{5}$$

A Poisson equation for the pseudo-pressure Π is obtained by applying a Divergence operator to the momentum equation (1), leading to

$$\nabla \cdot \nabla \Pi = -\nabla \cdot \nabla \cdot (\bar{\underline{u}} \otimes \bar{\underline{u}} + \tau^{\mathrm{D}}) \tag{6}$$

with

$$\tau^{\mathrm{D}} = \tau - \tfrac{1}{3}\,\mathrm{Tr}(\tau) I \tag{7}$$

2.2. Subgrid-scale models

All the SGS models studied in the present work belong to the eddy-viscosity family, and therefore assume a linear relationship between the deviatoric part of the subgrid tensor τ^{D} and the resolved stress tensor $\bar{S}$:

$$\tau^{\mathrm{D}} = -2\nu_{\mathrm{sgs}}\bar{S}, \quad \text{with } \bar{S} = \tfrac{1}{2}(\nabla \bar{\underline{u}} + \nabla^{\mathrm{T}} \bar{\underline{u}}) \tag{8}$$

where ν_{sgs} is the subgrid viscosity, which remains to be determined. Three basic models are considered here. They all depend exclusively on the resolved scales, and do not involve any additional transport equation. The subgrid viscosity appears then as a function of the cut-off lengthscale $\bar{\Delta}$ and the resolved velocity field $\bar{\underline{u}}$.

The Smagorinsky model [13] assumes the following dependency:

$$\nu_{\mathrm{sgs}}(\bar{\Delta}, \bar{\underline{u}}) = (c_1 \bar{\Delta})^2 \,|\, \bar{S} \,|, \quad |\, \bar{S} \,| = \sqrt{2 \bar{S}_{ij} \bar{S}_{ij}} \tag{9}$$

where the constant c_1 is taken equal to 0.18 for isotropic turbulence and is lowered to 0.1 for plane channel flow in Deardorff [14], and $\bar{\Delta}$ is the cut-off lengthscale. In the present computations, $\bar{\Delta}$ is evaluated as $\bar{\Delta} = (\Delta x \Delta y \Delta z)^{1/3}$.

The Structure Function model, as proposed by Métais and Lesieur [9], reads:

$$\nu_{\mathrm{sgs}}(\bar{\Delta}, \bar{\underline{u}}) = c_2 \bar{\Delta} \sqrt{\bar{F}_2(r)} \tag{10}$$

where c_2 is a constant equal to 0.063 and the second-order structure function of the resolved velocity field $\bar{F}_2(r)$ is calculated performing the following surface integration:

$$\bar{F}_2(r) = \int_{|x'|=r} |\, \bar{\underline{u}}(\underline{x} + \underline{x}') - \bar{\underline{u}}(\underline{x}) \,|^2 \, \mathrm{d}^2 s \tag{11}$$

The Mixed Scale model, as proposed by Sagaut [15], exhibits a triple dependency on the vorticity of the resolved scales $\bar{\omega}$, the kinetic energy of the highest resolved frequencies q_{c} and the cut-off lengthscale:

$$\nu_{\mathrm{sgs}}(\bar{\Delta}, \bar{\underline{u}}) = c_3 \,|\, \bar{\underline{\omega}} \,|^{1/2} q_{\mathrm{c}}^{1/4} \bar{\Delta}^{3/2}, \quad \bar{\underline{\omega}} = \nabla \times \bar{\underline{u}} \tag{12}$$

The value of the constant c_3 is 0.06. The quantity q_{c} represents the kinetic energy of the test field $\bar{\underline{u}}' = \bar{\underline{u}} - \tilde{\bar{\underline{u}}}$, which is extracted from the resolved velocity field through the application of a test filter associated to the cut-off lengthscale $\tilde{\bar{\Delta}} > \bar{\Delta}$ (hereafter represented by the *tilde*):

$$q_{\mathrm{c}} = \tfrac{1}{2}\, \bar{u}_i' \bar{u}_i' \tag{13}$$

These three models have originally been developed assuming that the simulated flow is turbulent, fully developed and isotropic in the whole computational domain, and *a priori* do not incorporate any information related to a possible departure of the simulated flowfield from these assumptions. To obtain an automatic adaptation of the model for inhomogeneous flows, where the basic versions of the models may lead to dramatic errors on the computed solution, two techniques have been employed in the present work, which are now briefly presented.

2.3. Dynamic models

The first solution is to use the Germano–Lilly [16, 17] dynamic procedure to compute the constant of the subgrid-viscosity model, leading to the definition of dynamic models. This procedure is based on the Germano identity, which links the subgrid tensor τ to the equivalent tensor obtained at another filtering level (the aforementioned test filter). Rewriting the relation (8) for the two filtering levels under the symbolic form:

$$\tau_{ij}^{\mathrm{D}} = C\alpha_{ij}(\underline{\bar{u}}, \bar{\Delta}), \quad T_{ij}^{\mathrm{D}} = C\alpha_{ij}(\underline{\tilde{\bar{u}}}, \tilde{\bar{\Delta}}) \tag{14}$$

where

$$\alpha_{ij} = \frac{-2\nu_{\mathrm{sgs}}\bar{S}_{ij}}{C} \tag{15}$$

the constant C of the eddy-viscosity model is computed as

$$C = \frac{m_{ij}L_{ij}}{m_{kl}m_{kl}} \tag{16}$$

with

$$m_{ij} = \alpha_{ij}(\underline{\tilde{\bar{u}}}, \tilde{\bar{\Delta}}) - \tilde{\alpha}_{ij}(\underline{\bar{u}}, \bar{\Delta}), \qquad L_{ij} = \widetilde{\bar{u}_i\bar{u}_j} - \tilde{\bar{u}}_i\tilde{\bar{u}}_j \tag{17}$$

The use of the dynamic procedure was shown to enable the definition of subgrid viscosities to vanish automatically in the near-wall region of wall bounded flows.

2.4. Selective models

Another possibility for designing self-adaptive SGS models is to combine a basic subgrid-viscosity model with a selection function, as originally proposed by David [8] and Lesieur and Métais [18]. This selection function, referred to as f_s, checks the structural properties of the test field $\bar{u}'$, and turns off the SGS model when these properties do not correspond to those expected from a fully turbulent field. In practice, a velocity field will be considered as turbulent and requiring a SGS (and the SGS model will be turned on) if the local angular fluctuation of the instantaneous filtered vorticity is higher than a given threshold angle θ_0 obtained by David [8] with a DNS in homogeneous isentropic turbulence. A pic is found in the neighbourhood of 20°.

Rather than the original Boolean selection function proposed by David [8], we use here the modified continuous selection function proposed in Sagaut and Troff [10] in order to prevent numerical problems:

$$f_s(\theta, \theta_0) = \begin{cases} 1 & \text{if } \theta \geqslant \theta_0 \\ r(\theta, \theta_0)^n & \text{else} \end{cases} \tag{18}$$

where the function r is defined as

$$r(\theta,\theta_0)=\frac{\tan^2(\theta/2)}{\tan^2(\theta_0/2)} \tag{19}$$

a priori tests show that the best value for n is $n=2$, the calculations presented hereafter have been performed using this value. Using the aforementioned notations, the modified SGS model reads:

$$\tau_{ij}^{\mathrm{D}}=C' f_{\mathrm{s}}(\theta,\theta_0)\alpha_{ij}(\bar{\underline{u}},\bar{\Delta}) \tag{20}$$

Following David's recommendation deduced from isotropic turbulence simulations, the constant is evaluated as $C'=1.65\times C$ in order to obtain the same domain-averaged mean value of the subgrid viscosity as for non-selective models, and the threshold angle θ_0 is taken equal to 20°.

3. NUMERICAL METHOD

3.1. Spatial discretization

The discretized Navier–Stokes equations are solved on a non-staggered grid. Discrete operators of the space-derivatives are evaluated after rewriting the continuous operators in generalized co-ordinates. Taking into account the fact that the grid is Cartesian in our case (i.e. $x_1=x_1(\xi_1), x_2=x_2(\xi_2), x_3=x_3(\xi_3)$, where (x_1,x_2,x_3) and (ξ_1,ξ_2,ξ_3) are the co-ordinates in physical and reference frames, respectively), we get:

$$\frac{\partial\phi}{\partial x_i}=\frac{1}{J}\frac{\partial}{\partial x_k}\left(J\frac{\partial\xi_k}{\partial x_i}\phi\right)=\frac{\partial\phi}{\partial\xi_i}\frac{\partial\xi_i}{\partial x_l}\delta_{il} \tag{21}$$

$$\frac{\partial^2\phi}{\partial x_i\partial x_j}=\frac{1}{J}\frac{\partial}{\partial\xi_l}\left(\frac{\partial\xi_l}{\partial x_j}\frac{\partial}{\partial\xi_k}\left(J\frac{\partial\xi_k}{\partial x_i}\phi\right)\right) \tag{22}$$

where $J=(\partial x_1/\partial\xi_1)(\partial x_2/\partial\xi_2)(\partial x_3/\partial\xi_3)$ is the Jacobian of the transformation.

Spatial derivatives are approximated using centred second-order accurate finite difference schemes. For first-order derivatives, the fully three-dimensional scheme presented in Lê *et al.* [19] is employed, which reduces the amplification of odd-even spurious modes. As an example, the derivative in the ξ_1 direction at the (i,j,k) node is approximated in the following way:

$$\begin{aligned}\left(\frac{\partial\phi}{\partial\xi_1}\right)_{i,j,k}=\frac{1}{72\Delta\xi_1}&(\phi_{i+1,j+1,k+1}-\phi_{i-1,j+1,k+1}+\phi_{i+1,j+1,k-1}-\phi_{i-1,j+1,k-1}\\&+\phi_{i+1,j-1,k+1}-\phi_{i-1,j-1,k+1}+\phi_{i+1,j-1,k-1}-\phi_{i-1,j-1,k-1}\\&+4(\phi_{i+1,j,k+1}-\phi_{i-1,j,k+1}+\phi_{i+1,j,k-1}-\phi_{i-1,j,k-1}\\&+\phi_{i+1,j-1,k}-\phi_{i-1,j-1,k}+\phi_{i+1,j+1,k}-\phi_{i-1,j+1,k})\\&+16(\phi_{i+1,j,k}-\phi_{i-1,j,k}))\end{aligned} \tag{23}$$

Following Kravenchko and Moin [20], the convection term is written in skew-symmetric form, in order to reduce the aliasing error and to improve the stability of the method, yielding:

$$\nabla\cdot(\bar{\underset{\sim}{u}}^n\otimes\bar{\underset{\sim}{u}}^n)=\frac{1}{2}(\nabla\cdot(\bar{\underset{\sim}{u}}^n\otimes\bar{\underset{\sim}{u}}^n)+\bar{\underset{\sim}{u}}^n\nabla\,\bar{\underset{\sim}{u}}^n) \tag{24}$$

Second-order derivatives are discretized using compact 3-point operators Lê *et al.* [19]. Examples are:

$$\frac{\partial}{\partial xi_1}\left(g\frac{\partial\phi}{\partial xi_1}\right)_{i,j,k}=\frac{1}{2\Delta\xi_1^2}(\phi_{i+1,j,k}(g_{i,j,k}+g_{i+1,j,k})-\phi_{i,j,k}(2g_{i,j,k}+g_{i+1,j,k}+g_{i-1,j,k}) + \phi_{i-1,j,k}(g_{i,j,k}+g_{i-1,j,k})) \tag{25}$$

$$\frac{\partial}{\partial xi_1}\left(g\frac{\partial\phi}{\partial xi_2}\right)_{i,j,k}=\frac{1}{4\Delta\xi_1\Delta\xi_2}(g_{i+1,j,k}(\phi_{i+1,j+1,k}-\phi_{i+1,j-1,k}) - g_{i-1,j,k}(\phi_{i-1,j+1,k}-\phi_{i-1,j-1,k})) \tag{26}$$

3.2. Time integration

Time integration is achieved using a second-order accurate semi-implicit method. Convection terms are treated using an explicit second-order Adams–Bashforth scheme, while the implicit second-order backward differentiation formula (BDF) is employed for the molecular diffusion term. A special treatment is used for the SGS terms, based on a splitting which uncouples the dispersive terms from the dissipative ones:

$$\begin{aligned}\nabla\cdot\tau&=\nabla\cdot(-\nu_{\mathrm{sgs}}(\nabla\bar{\underset{\sim}{u}}+\nabla^t\bar{\underset{\sim}{u}}))\\&=-\nabla\nu_{\mathrm{sgs}}\cdot(\nabla\bar{\underset{\sim}{u}}+\nabla^t\bar{\underset{\sim}{u}})-\nu_{\mathrm{sgs}}\nabla^2\bar{\underset{\sim}{u}}\end{aligned} \tag{27}$$

The first term of the right-hand side of Equation (27) has a dispersive character, and is treated explicitely like the convection term in order to preserve the conditioning of the implicit problem. The second term is treated implicitely, like the molecular diffusion, in order to improve the numerical stability. Because the SGS viscosity appears as a strongly non-linear function of the resolved quantities, it was chosen to use a first-order accurate linearization for that term. The incompressibility constraint is enforced using an approximate projection method in Lê *et al.* [19]. The resulting semi-discretized problem, written for the incremental unknown $\Delta\,\underset{\sim}{u}^n=\underset{\sim}{u}^{n+1}-\underset{\sim}{u}^n$, reads:

$$\left[1-\frac{2\Delta t}{3}\left(\frac{1}{Re}+\nu_{\mathrm{sgs}}^n\right)\nabla^2\right]\Delta\underset{\sim}{u}^n=\frac{1}{3}\Delta\underset{\sim}{u}^{n-1}+\frac{2\Delta t}{3}\left\{\left(\frac{1}{Re}+\nu_{\mathrm{sgs}}^n\right)\nabla^2\underset{\sim}{u}^n-\nabla\Pi^n + (2\nabla\nu_{\mathrm{sgs}}:\bar{S})^*-(\nabla\cdot(\bar{\underset{\sim}{u}}\otimes\bar{\underset{\sim}{u}}))^*\right\} \tag{28}$$

where the *star* refers to the second-order Adams–Bashforth extrapolation:

$$\phi^*\equiv 2\phi^n-\phi^{n-1} \tag{29}$$

The pseudo-pressure Π^n is computed by solving the following semi-discrete Poisson equation:

$$-\nabla^2\Pi^n = \nabla\cdot\nabla\cdot(\underline{\underline{\bar{u}}}^n\otimes\underline{\underline{\bar{u}}}^n + (\tau^{\mathrm{D}})^n) - \frac{2}{\Delta t}\nabla\cdot\underline{\underline{\bar{u}}}^n + \frac{1}{2\Delta t}\nabla\cdot\underline{\underline{\bar{u}}}^{n-1} \tag{30}$$

All linear systems coming from both the momentum and the Poisson equation are solved using the Bi-CGSTAB algorithm proposed by van der Vorst [21]. The problem associated to the Poisson equation with Neumann and periodic boundary conditions being ill-posed (see for example Strikwerda [22]), the additional constraint that the pressure has a zero mean value is imposed to recover a well-behaved problem.

Following the algorithm proposed by Deschamps [23], a time-adaptive homogeneous forcing term, $F_1(t)$, is added to the momentum equation in order to keep a constant mass flux across the channel. The bulk velocity is given by the following relation:

$$\bar{u}_{\mathrm{b}} = \frac{1}{L_z}\int_0^{L_z}\langle\bar{u}\rangle_{xy}\,\mathrm{d}z \tag{31}$$

where $\langle.\rangle_{xy}$ operator stands for averaging over the xy plane, L_z is the width of the channel. Integrating the result in the wall-normal direction, one obtains a time-dependent equation for the bulk velocity, $\bar{u}_{\mathrm{b}}$:

$$\begin{aligned}\frac{\mathrm{d}\bar{u}_{\mathrm{b}}}{\mathrm{d}t} + \underbrace{\frac{1}{L_z}\int_0^{L_z}(\langle\bar{u}\bar{w}\rangle_{xy} + \langle\tau_{13}\rangle_{xy})\,\mathrm{d}z}_{=0} \\ = -\frac{1}{L_z}\int_0^{L_z}F_1(t)\,\mathrm{d}z + \frac{1}{L_z}\int_0^{L_z}\frac{1}{Re}\frac{\partial^2}{\partial z\partial z}\langle\bar{u}\rangle_{xy}\,\mathrm{d}z\end{aligned} \tag{32}$$

This equation can be written as follows:

$$\frac{\mathrm{d}\bar{u}_{\mathrm{b}}}{\mathrm{d}t} = \underbrace{-F_1(t) + \frac{1}{L_z}\left[\frac{1}{Re}\frac{\partial}{\partial z}\langle\bar{u}\rangle_{xy}\right]_0^{L_z}}_{S(t)} \tag{33}$$

The second term of right-hand side corresponds to the square of the wall friction velocity. Supposing the forcing term $\tilde{F}_1^{(n)}$ at time step n is known then $\tilde{F}_1^{(n+1)}$ is computed using the relation:

$$\tilde{F}_1^{(n+1)} = \tilde{F}_1^{(n)} + \alpha(\tilde{u}_{\mathrm{b}}^{(n+1)} - \tilde{u}_{\mathrm{b}}^{(0)}) + \beta(\tilde{u}_{\mathrm{b}}^{(n)} - \tilde{u}_{\mathrm{b}}^{(0)}) \tag{34}$$

where $\tilde{u}_{\mathrm{b}}^{(0)}$, $\tilde{u}_{\mathrm{b}}^{(n)}$ and $\tilde{u}_{\mathrm{b}}^{(n+1)}$ are, respectively, the bulk velocity (supposed to be conserved), the bulk velocity at time step n and a first-order predictor of the bulk velocity at time step $n+1$ given by

$$\tilde{u}_{\mathrm{b}}^{(n+1)} = \tilde{u}_{\mathrm{b}}^{(n)} + \Delta t\tilde{S}^{(n)} \tag{35}$$

A stability analysis shows that the algorithm is more efficient for $\alpha = 1$ and $\beta = -0.5$.

3.3. SGS model implementation

Because no explicit information about the location of the wall is used for the parametrization of the subgrid terms, fully three-dimensional versions of the selected SGS models are employed: the 3D Structure Function is implemented, as described in Comte *et al.* [24], and a 3D test filter serves as a basis to evaluate the test field $\tilde{u}'$. This test filter results from the tensorial product of the following 1D discrete filter:

$$\tilde{\phi}_l = \tfrac{1}{6}(\phi_{l-1} + 4\phi_l + \phi_{l+1}) \tag{36}$$

The characteristic lengthscale of this filter is equal to $2\Delta x$ [25].

As usual, the dynamic model needs to be stabilized to carry out the simulation. A plane averaging procedure of both the denominator and the numerator of the dynamic constant is used.

3.4. Boundary conditions

Periodic boundary conditions are used for the pressure and the velocity in directions parallel to the walls, i.e. x and y. No-slip conditions are imposed on the velocity field at the solid walls. Following Gresho [26], a natural boundary condition obtained by considering the momentum equation in the wall-normal direction is used for the pressure.

4. CHARACTERISTICS OF THE SIMULATIONS

Simulations were performed at $Re_\tau = 180$ and 395 ($Re_\tau = u_\tau \delta / \nu$, $u_\tau = \sqrt{\tau_w/\rho}$ being the friction velocity, δ the channel half-width and ν the kinematic viscosity), on two grids for each case. These values of the friction Reynolds number correspond to the DNS data base of Kim *et al.* [11] and Mansour *et al.* [12], which will be used for validation. Computational parameters are given in Table I for $Re_\tau = 180$ and in Table II for $Re_\tau = 395$.

Based on previous DNS and LES, the size of the computational domain is taken equal to $Lx = 4\pi$ and $Ly = \pi$, which, for all the considered cases, ensures that two-point correlations in these two directions are negligible for separation distance of the order of a half of the computational domain size. The mesh is uniform in homogeneous directions, and is distributed following a hyperbolic tangent law in the wall normal direction.

Table I. Configuration and mesh characteristics for the current simulations ($Re_\tau = 180$). Symbol '+'refers to wall units. For DNS computations the first number of grid point corresponds to reference simulations, while the number in parentheses corresponds to the number of grid points required to mesh the current computational domain with the same resolution.

				$Lx = 4\pi\delta$ $Lx^+ = 2262$	$Ly = \pi\delta$ $Ly^+ = 566$	$Lz = 2\delta$ $Lz^+ = 360$
	m_x	m_y	m_z	Δx^+	Δy^+	$\min(\Delta z^+)$
Fine mesh	64	64	67	35	8.8	1
Coarse mesh	32	32	67	71	17.6	1
Kim *et al.*	128 (188)	128 (80)	129	12	7	0.05

Table II. Configuration and mesh characteristics for the current simulations ($Re_\tau = 395$). Symbol '+' refers to wall units. For DNS computations the first number of grid point corresponds to reference simulations, while the number between parentheses would correspond to the number of grid points required to mesh the present computational domain with the same resolution.

				$Lx = 4\pi\delta$ $Lx^+ = 4963$	$Ly = \pi\delta$ $Ly^+ = 1252$	$Lz = 2\delta$ $Lz^+ = 790$
	m_x	m_y	m_z	Δx^+	Δy^+	$\min(\Delta z^+)$
Fine mesh	64	64	67	78.4	18.4	1
Coarse mesh	32	32	67	156.8	36.8	1
Mansour *et al.*	256 (497)	192 (192)	193 (193)	10	6.5	0.05

The time unit t^+ is based on the friction velocity and the molecular viscosity by

$$t^+ = \frac{t\, u_\tau^2}{\nu} \tag{37}$$

The time step Δt is chosen such that $\Delta t^+ = 9.81 \times 10^{-3}$ and 1.97×10^{-2}, respectively, for the $Re_\tau = 180$ and 395 cases, ensuring a good temporal representation of the near-wall dynamics.

The time-filtering effects due to time discretization are then assumed to be negligible compared to the spatial filtering ones.

For each case, the following four SGS models are used: dynamic Smagorinsky (Sdyn), selective versions of the Smagorinsky model (Sslc), the Structure Function model (SFslc) and the Mixed Scale model (MSslc). A coarse-resolution simulation (DNSc), i.e. a simulation without an SGS model, is also performed in each case to check the relative influence of the SGS terms on the results.

Statistical moments have been computed by performing an averaging in both time and homogeneous directions. It was checked that all the results are fully averaged over long enough time. At least 10^8 samples, collected over a non-dimensional time equal to 6 cross-channel times, were used. The statistical average is noted by brackets $\langle\,\rangle$.

5. VALIDATION

LES calculations are first validated by performing comparisons of results for the mean velocity field and typical turbulent quantities with DNS data of Kim *et al.* [11] for the $Re_\tau = 180$ case, and with DNS data of Mansour *et al.* [12] for the $Re_\tau = 395$ case. Because the effective filter of the LES simulations, i.e. its exact characteristic lengthscale and mathematical expression, remains unknown, it was chosen to use DNS data without filtering or defiltering LES data. As stated by Härtel and Kleiser [4] and Winckelmans *et al.* [27], such comparisons are meaningful when dealing with quantities derived from the mean velocity profile, but may induce some erroneous conjectures when applied to turbulent quantities, because of unresolved turbulent fluctuations. DNS data will then be considered as target values for LES computations when

Table III. Computed relative error (in %) on the friction velocity u_τ and mean centreline velocity U_c, with respect to DNS data.

	u_τ				U_c			
	$Re_\tau = 180$		$Re_\tau = 395$		$Re_\tau = 180$		$Re_\tau = 395$	
	Coarse	Fine	Coarse	Fine	Coarse	Fine	Coarse	Fine
DNSc	+13	+15	+2.8	+15	−4.6	−3.9	−5.8	−4.9
Sdyn	+9.4	+15	+3	+12	−4.6	−3.6	−5.4	−3.8
Sslc	+1.1	+5.6	−22	−9	−3.7	−3.8	−5	−3
SFslc	+4.4	+12	−5	+5	−3.2	−3.1	−5.1	−3.6
MSslc	−2.8	+1.7	−18	−9.5	−3.8	−3.1	−4.3	−3.8

dealing with the mean velocity field, but not when considering the higher order statistical moments.

5.1. Mean velocity field

The quality of the recovery of DNS results at the wall and the centreline is first evaluated. Relative errors with DNS value of the friction velocity u_τ and mean centreline velocity U_c for all cases are summarized in Table III. Because they are sensitive to different features of the SGS models, these quantities will be discussed separately.

A look at the error on U_c reveals that the centreline velocity is underpredicted within 3–5% for all cases, leading to a satisfactory agreement. Zahrai *et al.* [28] reported a very similar error level at $Re_\tau = 180$ using an anisotropic Smagorinsky model for grid resolutions corresponding to the present medium resolution: from −5.26% with $(\Delta x^+ = 70.7, \Delta y^+ = 8.8)$ to −1.68% with $(\Delta x^+ = 70.7, \Delta y^+ = 17.7)$. Overestimation up to 10% of the centreline velocity is also reported by these authors when the viscous sublayer is not resolved, with a first mesh point located at $z^+ = 5$. A comparable error range (1–5%) is observed by Härtel and Kleiser [4] using an optimized Smagorinsky model at three Reynolds numbers ($Re_\tau = 115, 210$ and 300) with a resolution comparable to the present medium resolution $(\Delta x^+ = 80, \Delta y^+ = 30)$. But it is to be noticed that a systematic overprediction was observed in these simulations. The factor responsible for that discrepancy remains unclear, because of the lack of published related studies. At a given Reynolds number, whatever SGS model is used, grid refinement is found to improve the results, but the use of a SGS model does not always lead to an improvement of the coarse grid DNS results. This is in agreement with the conclusion of Härtel and Kleiser [9], while worst results were surprisingly obtained when refining the grid in the spanwise direction by Zahrai *et al.* [28], maybe due to the high level of grid anisotropy.

Results concerning the friction velocity are less satisfactory than those obtained on the centreline velocity.

For the $Re_\tau = 180$ case, a general trend to overpredict this quantities is observed, the highest value being obtained with the DNSc simulation. The same overprediction in coarse-grid DNS carried out with non-dissipative numerical schemes is also reported by Härtel and Kleiser [4] (15% error on the wall stress τ_w for their three Reynolds numbers), by Sarghini *et al.* [29] (6% error for $Re_\tau = 180$, with $\Delta x^+ = 35.5, \Delta y^+ = 15.7$, and 18% error for $Re_\tau = 1050$ with $\Delta x^+ = 103, \Delta y^+ = 25.8$), and by Najjar and Tafti [25] (<3% error for $Re_\tau = 180$, with same

resolution as the present fine grid case). This phenomena is due to the fact that coarse grid DNS does not account for the net resolved energy drain toward the SGS scales, resulting in increased turbulence fluctuations and in steeper velocity profiles at the wall. The numerical method may have a deep impact on the result of coarse grid DNS: Najjar and Tafti have demonstrated that upwind biased scheme DNS leads to an underprediction of the wall stress, like the second-order centred scheme on staggered mesh used in Sagaut and Troff [10] did on a ($\Delta x^+ = 72, \Delta y^+ = 24$) grid at $Re_\tau = 180$. The latter author also reported that the use of a finer grid ($\Delta x^+ = 36, \Delta y^+ = 12$) with its second-order method or the use of a spectral method permit to recover the classical overprediction of the shear stress. This shows that the present non-staggered grid algorithm provides less intrisic damping than the staggered one of Sagaut and Troff [10].

It was observed in Zahrai *et al.* [28] and in Najjar and Tafti [25] that the addition of a SGS dissipation leads to a decrease of the wall stress. The general overprediction of the wall stress in all the present simulations (except the MSslc-coarse grid simulation) indicates that the SGS models are underpredicting the exact SGS dissipation rate $\varepsilon = -\tau_{ij}\bar{S}_{ij}$. Different behaviours can also be observed for low Reynolds number LES ($Re_\tau \leqslant 300$): Sarghini and Piomelli reported a general trend to underpredicting the wall stress when using Smagorinsky and non-Lagrangian dynamic models at $Re_\tau = 180$, the optimized Smagorinsky model of Härtel and Kleiser leads to underprediction within 9–14% of the friction velocity, depending on the Reynolds number, and an underprediction of 18% of the friction coefficient $c_f = 2\tau_w/u_b^2$ (u_b being the bulk velocity) at $Re_\tau = 180$ is reported in David [8]. But it is important to notice that, at high Reynolds number ($Re_\tau = 1050$), a trend to large overprediction of the friction velocity within 16–20% is reported by Sarghini and Piomelli using various dynamic models. Several causes can be invoked to explain these discrepancies: numerical scheme, resolution (i.e. computational grid), SGS model and stabilization procedure for dynamic models, and the discrete test filter for multi-level SGS models [25, 30].

Different behaviours are observed on the $Re_\tau = 395$ case: some SGS models are now leading to underprediction of the wall stress, with level error as high as -22% (Sslc, coarse grid), while others are still overpredicting it. Unlike the low Reynolds number case, some SGS models may lead to higher values of the friction velocity than the DNSc simulations. The same observation is reported in Sarghini *et al.* [29], using a dynamic model together with a top-hat test filter at $Re_\tau = 1050$. This illustrates the fact that, by modifying the turbulent grid scale dissipation, the SGS models can also affect the mean velocity profile and the turbulent grid scale production, and hence generate steeper velocity profile near the wall, leading to a higher error level on the wall stress.

Grid refinement is not found to lead to a systematic improvement on the quality of the prediction of the friction velocity. For the $Re_\tau = 180$ case, it is shown to induce an increase of the skin friction, whatever SGS model is considered, indicating the existence of steeper gradient at the wall. This is consistent with the LES basic assumption that a finer grid corresponds to an higher cut-off frequency, then to smaller SGS stresses and a reduced subgrid viscosity. For SGS models which were found to be underdissipative on the coarse grid, results are found to be worst on the fine grid. An explanation for that fact may be that SGS models are not adaptating in a proper way to grid refinement in the near wall region: the SGS dissipation is found to decrease too fast. Same trends are observed at $Re_\tau = 395$, but, for the SGS models which are overdissipative the coarse grid, lowering the SGS dissipation by refining the grid results in an improvement of the data.

For filtered and dynamic models, an increase of the Reynolds number is observed to lead to a better prediction of the friction velocity, when performing coarse grid/coarse grid and fine grid/fine grid comparisons. This does not seem to be a general property of dynamic models, since Sarghini and Piomelli reported a clear degradation of the results when increasing the Reynolds number and coarsening the grid. Comparative analysis of the two medium resolution cases (fine grid at $Re_\tau = 395$ and coarse grid at $Re_\tau = 180$) does not permit to exhibit an obvious overall improvement of the results. But, with the exception of MSslc, the levels of error are very close for these two cases. This is to be compared with the conclusion of Härtel and Kleiser, who found that increasing the Reynolds number, while keeping the same frequency cut-off, yields an improvement of the results using their optimized Smagorinsky model. Several explanations for that discrepancy can be thought of: numerical accuracy (second-order Finite Differences in present case, spectral-Chebyshev in Härtel and Kleiser [9]), Reynolds numbers ($Re_\tau \leqslant 300$), and the fact that the Smagorinsky constant in Härtel *et al.* [10] was optimized in each case using DNS data rather than being taken equal to a unique value or automatically adjusted using a given self-adaptation procedure. Nevertheless, present results show that SGS models seem to at least keep the accuracy at a given grid resolution (expressed in wall units) when the Reynolds is increased. As already stated by previous authors Härtel *et al.* [2] and Piomelli *et al.* [3], the main issue here is the description of the coherent motion in the near wall region, which is associated to the production/dissipation of both grid scale and SGS fluctuations.

Mean centreline velocity is found to be more accurately predicted than friction velocity, whatever SGS model is considered, in a most consistent way, i.e. grid refinement leads to an improvement of the results. This is in agreement with conclusions of Härtel and Kleiser [4], that dissipative SGS models perform better in the core of the channel than in the near wall region, because turbulence is here in equilibrium, and that results on near wall flow and core flow are uncoupled thanks to the existence of the logarithmic regime in the boundary layer.

Figures 1–4 compare the mean streamwise velocity profiles in wall co-ordinates for the different computations. In agreement with Härtel and Kleiser [4], DNS and LES results compare satisfactorily within the viscous sublayer ($z^+ \leqslant 5$) in all cases, while large discrepancies are observed for $z^+ \geqslant 10$ at $Re_\tau = 180$ and $z^+ > 5$ at $Re_\tau = 395$. These discrepancies are mostly due to the error on the friction velocity. No SGS model is found able to recover the correct slope in the logarithmic layer, even at the highest Reynolds number on the fine grid. The same conclusion was drawn by Najjar and Tafti for $Re_\tau = 180$ and Härtel and Kleiser for $Re_\tau \leqslant 300$. The right slope value was obtained in Härtel and Kleiser [4] only by artificially lowering the SGS dissipation in an *ad hoc* way. It was also recovered naturally by Sarghini *et al.* in all their simulations at $Re_\tau = 1050$. These results are consistent with Antonia *et al.* [31] finding that low-Reynolds effects prevent the developement of a complete logarithmic layer in channel flow when $\delta^+ < 1000$.

5.2. *Turbulent quantities*

Profiles of the resolved turbulent stresses are presented in Figures 5–8. As usual, results are referred to the computed friction velocity.

The analysis of the results related to the resolved streamwise turbulence intensity reveals that all the computations yield the same qualitative behaviour: the turbulent stress admits a maximum located near $z^+ = 12$, in good agreement with DNS results. The value of the peak is

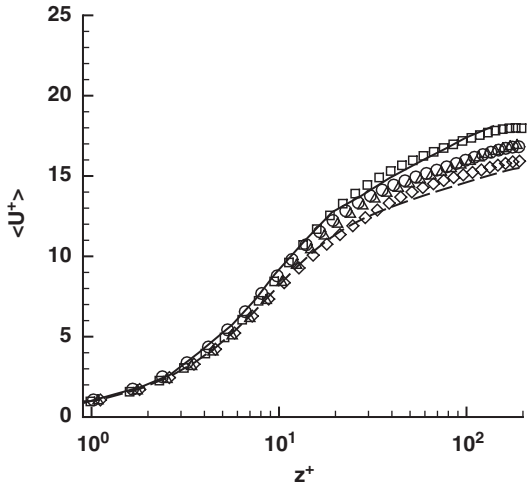

Figure 1. $Re_\tau = 180$. Mean Velocity profile normalized by the friction velocity—coarse grid. Dashed line: no model (coarse-resolution simulation), square: selective Mixed Scale model, triangle: selective Structure Function model, circle: selective Smagorinsky model, diamond: dynamic model with 3D test filter, full line: DNS data.

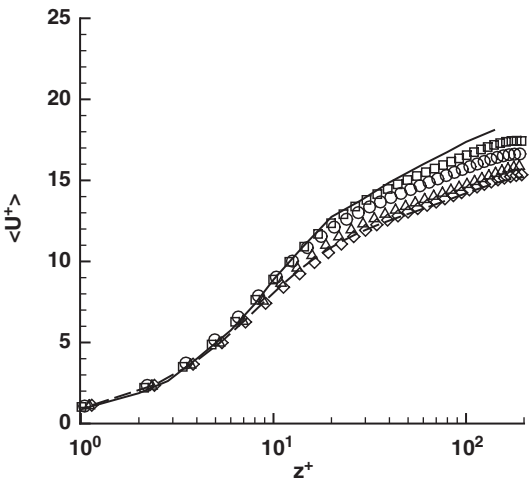

Figure 2. $Re_\tau = 180$. Mean velocity profile normalized by the friction velocity—fine grid. Caption: see Figure 1.

observed to depend strongly on the SGS model, the grid resolution and the Reynolds number. Generally speaking, the lowest values are obtained using the dynamic Smagorinsky model. This can be only partially explained by the observed trend to over-predict the skin friction with that model, showing that its use lead to a lower level of fluctuations. Results obtained

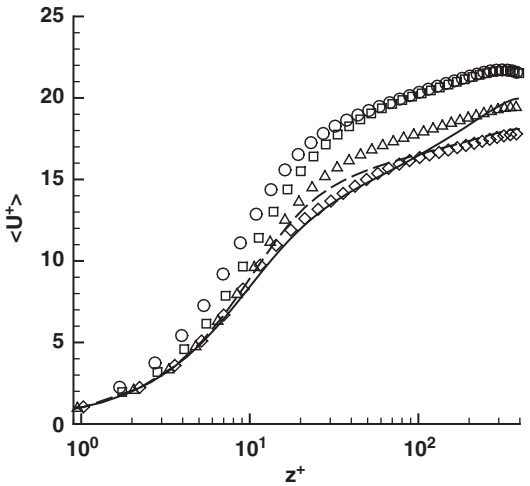

Figure 3. $Re_\tau = 395$. Mean velocity profile normalized by the friction velocity—coarse grid. Caption: see Figure 1.

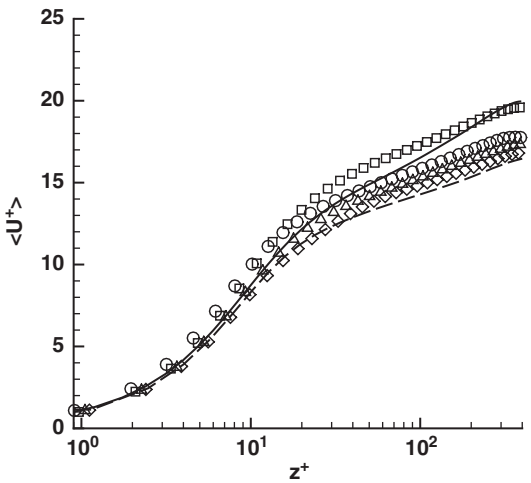

Figure 4. $Re_\tau = 395$. Mean velocity profile normalized by the friction velocity—fine grid. Caption: see Figure 1.

with the various combinations of subgrid model, computational grid and Reynold number do not make it possible to rank the models. But the general conclusion can be drawn from this results that the selective function yields physical results whatever basic formulation for the subgrid viscosity is used. This results are very similar to those obtained using a dynamic Smagorinsky model.

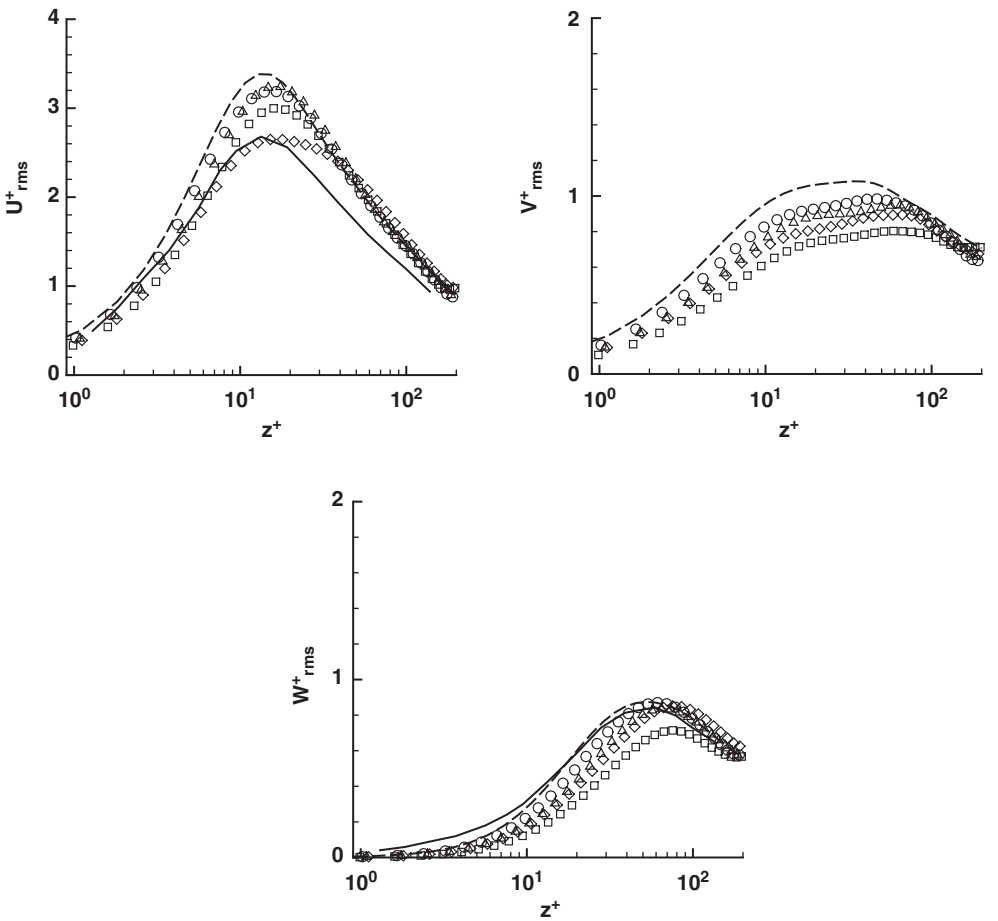

Figure 5. $Re_\tau = 180$. Resolved turbulent stresses normalized by the friction velocity—coarse grid. Caption: see Figure 1.

6. ANALYSIS OF THE SGS MODELS

The new selective subgrid models proposed in the present papers are now assessed by looking at their behaviour in the near-wall region. For sake of brevity, only results related to the $Re_\tau = 395$ case are reported below.

6.1. Mean value of the SGS viscosity

A deeper insight into the SGS model behaviour in the near-wall region is obtained by looking at the subgrid viscosity itself. Mean SGS viscosity profiles, shown in logarithmic co-ordinates, are plotted on Figures 9 and 10.

All the simulations exhibit the same qualitative behaviour, in agreement with those obtained with dynamic models by Najjar and Tafti [25] and Cabot [32]: the SGS viscosity is almost null

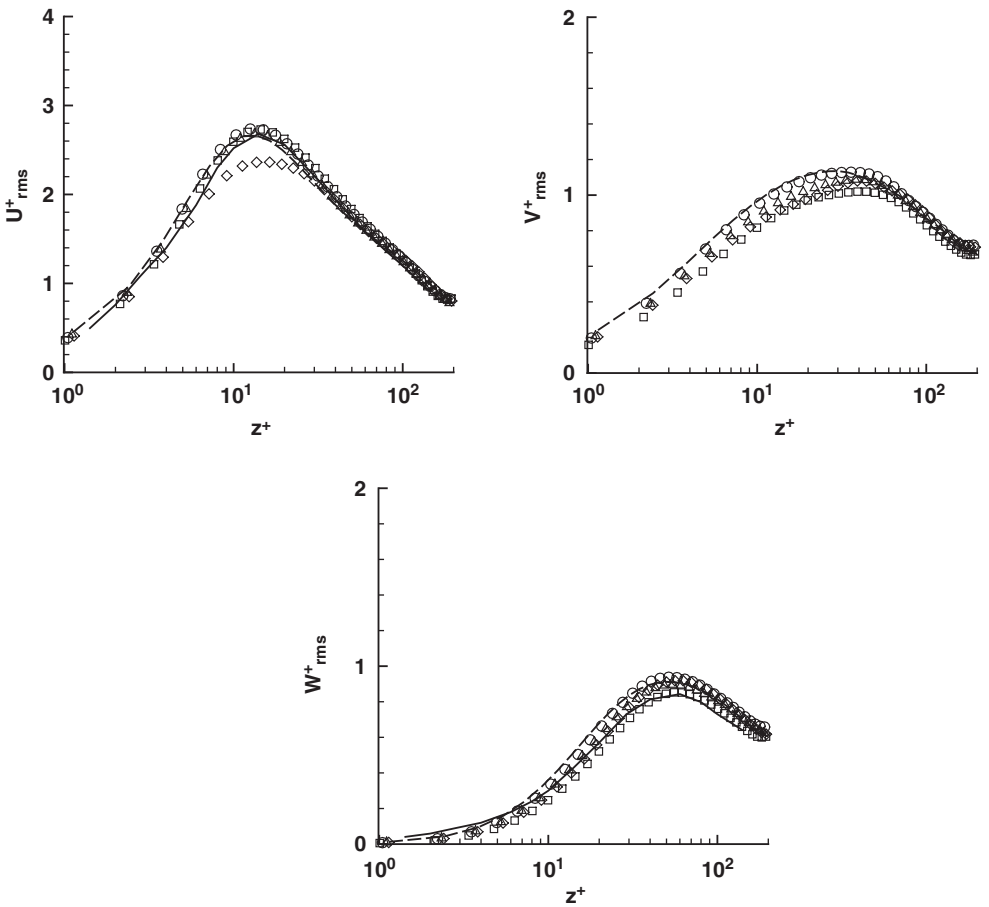

Figure 6. $Re_\tau = 180$. Resolved turbulent stresses normalized by the friction velocity—fine grid. Caption: see Figure 1.

at the solid wall, increases up to a maximum located in the buffer region, and then decreases when approaching the core region of the channel. Selective models are observed to decrease faster than the dynamic model for $z^+ < 10$, resulting in negligible values in that region. It is worth noting that the spectral dynamic model proposed by Lamballais *et al.* [33], which is based on the evaluation of the local slope of the energy spectrum, has the same properties. The present results seem to indicate that the quality of the results is not directly linked to the ability of the SGS viscosity to scale as z^{+3} in the near wall region, but to decrease quickly enough in that region to allow a good representation of the streaks. Some selective models exhibit a cusp behaviour at the wall, which is due to the definition of boundary conditions for the test filter at the solid wall. But this cusp is observed to be of negligible amplitude, and thus does not induce any problem.

The self-adaptation of subgrid viscosities is due to the selective function, which appear to yield a very significant improvement over the basic versions of the subgrid models. This is

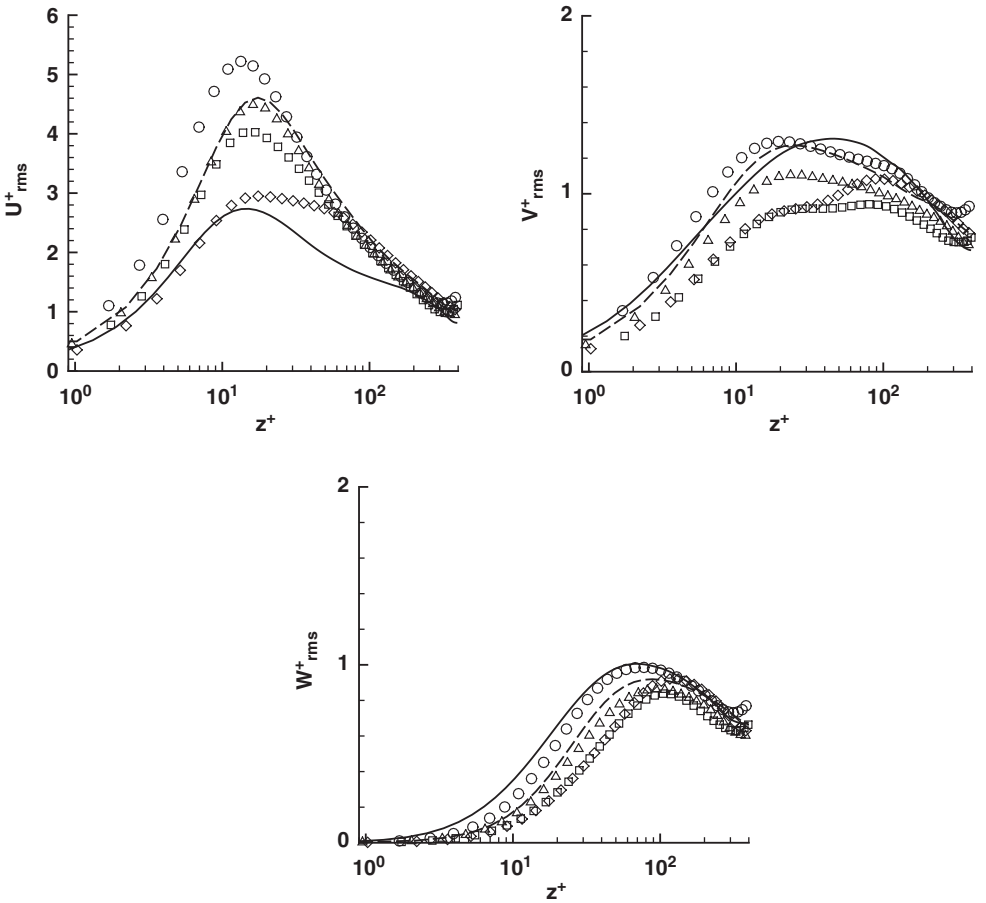

Figure 7. $Re_\tau = 395$. Resolved turbulent stresses normalized by the friction velocity—coarse grid. Caption: see Figure 1.

clearly seen by looking at the wall-value of the SGS viscosity associated to the mean velocity field. A second-order Taylor series expansion of the discretized versions of these models yields:

$$\nu_{\text{sgs}}|_{\text{w}} \simeq \sqrt{2}(c_1\bar{\Delta}|_{\text{w}})^2 \left|\frac{\partial\langle u\rangle}{\partial z}\right|_{\text{w}} \quad \text{Smagorinsky}$$

$$\nu_{\text{sgs}}|_{\text{w}} \simeq c_2\bar{\Delta}|_{\text{w}}\Delta z_1 \left|\frac{\partial\langle u\rangle}{\partial z}\right|_{\text{w}} \quad \text{Structure Function}$$

$$\nu_{\text{sgs}}|_{\text{w}} \simeq c_3\left(\frac{\sqrt{2}}{12}\right)^{1/2} \bar{\Delta}|_{\text{w}}^{3/2}\Delta z_1 \left|\frac{\partial\langle u\rangle}{\partial z}\right|_{\text{w}}^{1/2} \left|\frac{\partial^2\langle u\rangle}{\partial z^2}\right|_{\text{w}}^{1/2} \quad \text{Mixed Scale} \tag{38}$$

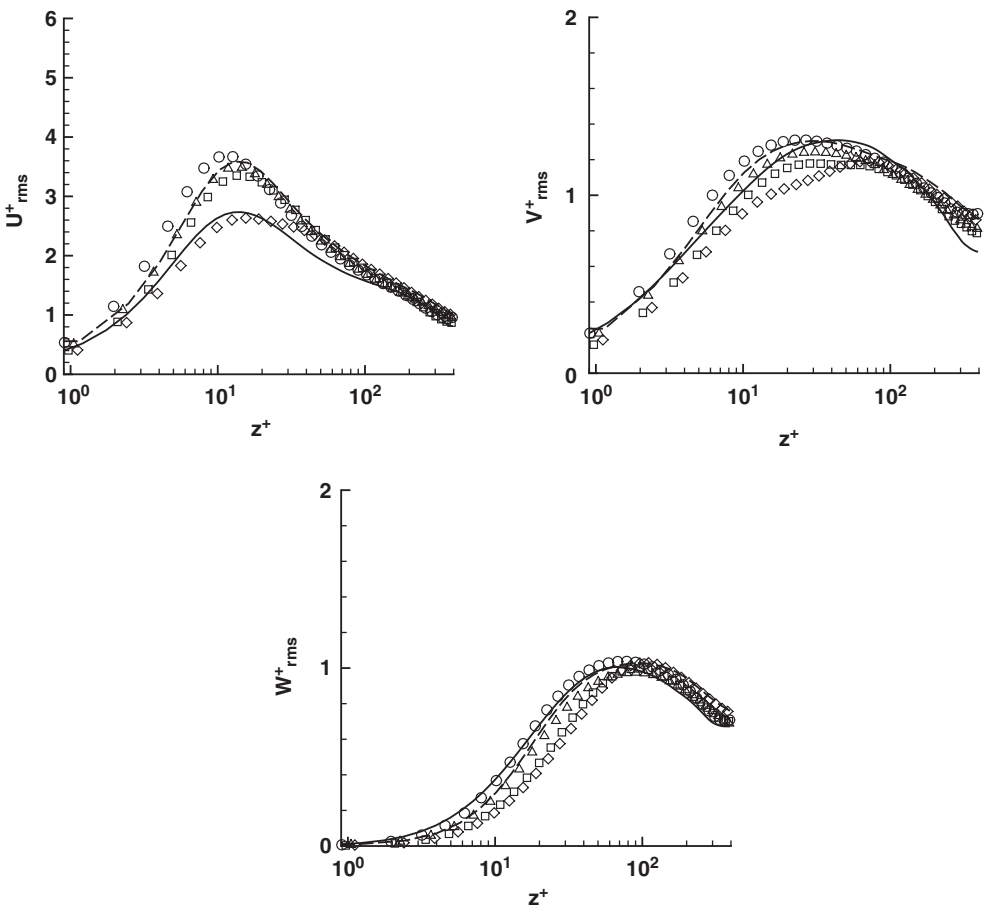

Figure 8. $Re_\tau = 395$. Resolved turbulent stresses normalized by the friction velocity—fine grid. Caption: see Figure 1.

where the subscript w denotes values taken at the wall, and Δz_1 is the height of the first mesh near the wall. Because the skin friction is non-zero at the wall (separation does not occur in that flow), the first two models are strictly non-vanishing at the solid boundaries. The Mixed Scale model could predict a zero SGS viscosity at the wall if at least the three first points were located in the region where the mean velocity profile obeys a linear law (the computed second-order derivative term would then be equal to zero). The computed values of the SGS viscosity demonstrate that the selective function acts as a wall-damping function, while it does not rely on any information related to the solid walls. The mean profile of the selection function is presented in Figures 11 and 12.

The mean value of the selection function is very small for $z^+ < 10$ in all the cases, providing the desired damping of the subgrid viscosity. This can be explained by the fact that the grid resolution is fine enough to permit a very good direct representation of the near-wall coherent structures, resulting in low values of the local angular fluctuation θ. Outside this region, the

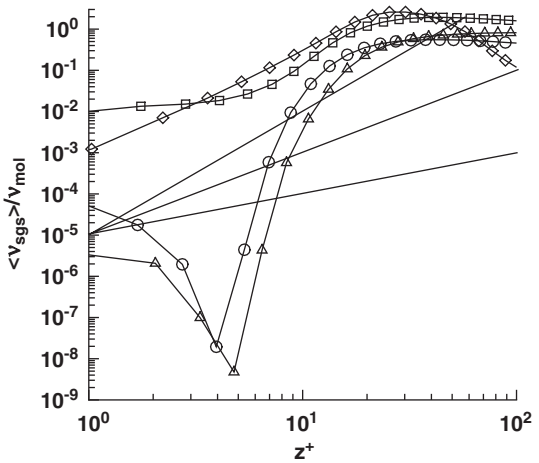

Figure 9. $Re_\tau = 395$. Normalized SGS viscosity profile normalized by the friction velocity—coarse grid. Caption: see Figure 1—solid straight lines show z^{+2}, z^{+3} and z^{+4} slopes.

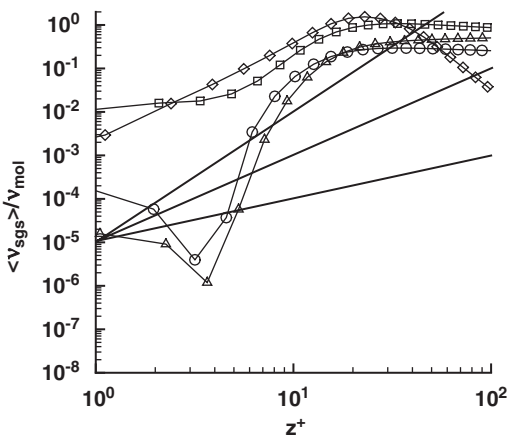

Figure 10. $Re_\tau = 395$. Normalized SGS viscosity profile normalized by the friction velocity—fine grid. Caption: see Figure 1—solid straight lines show z^{+2}, z^{+3} and z^{+4} slopes.

selection function exhibits a rapid growth, associated to a growing three-dimensionality of the highest resolved frequencies. This growth is the result of (i) the filling of the kinetic energy spectrum as the wall effects are weakening and (ii) the coarsening of the grid resolution in the wall-normal direction.

6.2. Subgrid dissipation

We now present results dealing with the SGS dissipation, $\varepsilon = -\tau_{ij}\bar{S}_{ij}$, which is a better indicator than the SGS viscosity to analyse the effect of the model on the computation. As proposed

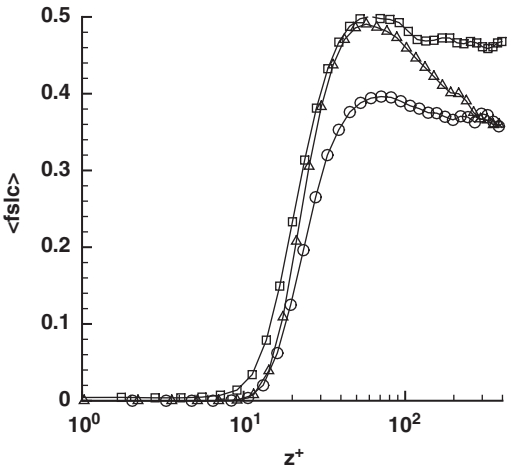

Figure 11. $Re_\tau = 395$. Mean profile of the selection function—coarse grid. Caption: see Figure 1.

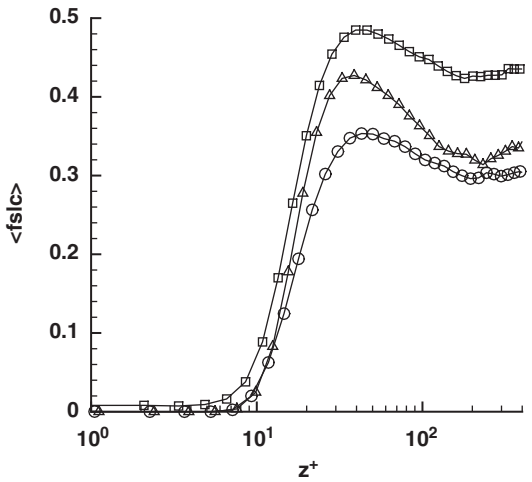

Figure 12. $Re_\tau = 395$. Mean profile of the selection function—fine grid. Caption: see Figure 1.

in Härtel *et al.* [2], it is split into the sum of the dissipation related to mean strain $\varepsilon_{\mathrm{MS}}$ and the redistribution of kinetic energy within the turbulence spectrum $\varepsilon_{\mathrm{FS}}$:

$$\langle \varepsilon \rangle = \langle \varepsilon_{\mathrm{MS}} \rangle + \langle \varepsilon_{\mathrm{FS}} \rangle, \langle \varepsilon_{\mathrm{MS}} \rangle = -\langle \tau_{ij} \rangle \langle \bar{S}_{ij} \rangle, \langle \varepsilon_{\mathrm{FS}} \rangle = -\langle \tau''_{ij} \bar{S}_{ij}{}'' \rangle \tag{39}$$

where the fluctuating part of a dummy variable ϕ is defined as $\phi'' = \phi - \langle \phi \rangle$. Mean profiles of these two quantities normalized by the bulk velocity, the molecular viscosity and the channel height in the wall-normal direction are plotted in Figures 13 and 14.

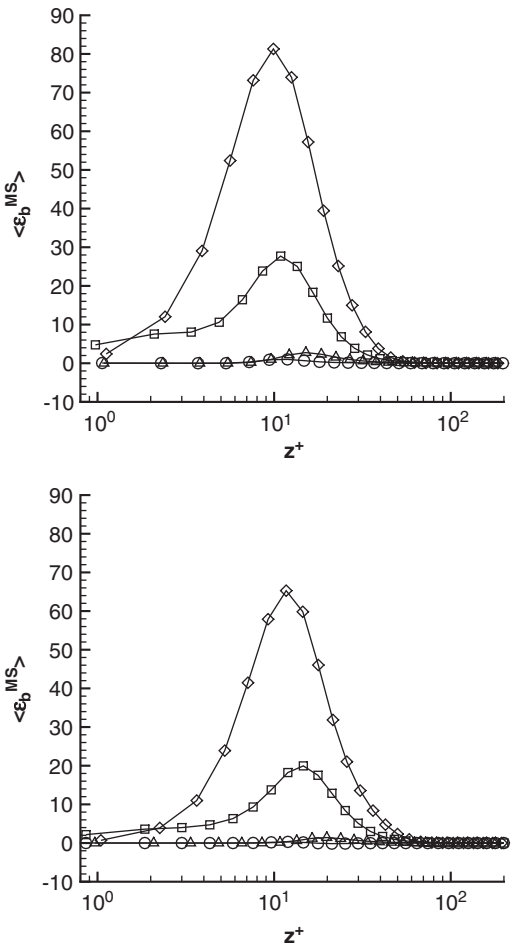

Figure 13. Mean strain SGS dissipation $\langle \varepsilon_{MS} \rangle$ profile normalized by the bulk velocity, the molecular viscosity and the channel height on the fine (top) and coarse (bottom) grid. Caption: see Figure 1.

A strong influence of both the basic SGS model and the adaptation procedure is observed on the amplitude of ε_{MS}, but some general features are common to all the simulations, which are all in good agreement with *a priori* tests of Härtel *et al.* [2, 4]:

- The mean strain dissipation is decreasing for $z^+ < 10$, due to the damping provided by the self-adaptation procedure.
- The mean strain dissipation exhibits a maximum in the buffer region ($10 \leqslant z^+ \leqslant 20$).

A very interesting result is seen by looking at the fluctuating strain dissipation profile: some negative values are clearly recovered on the coarse grid when using the selective Mixed

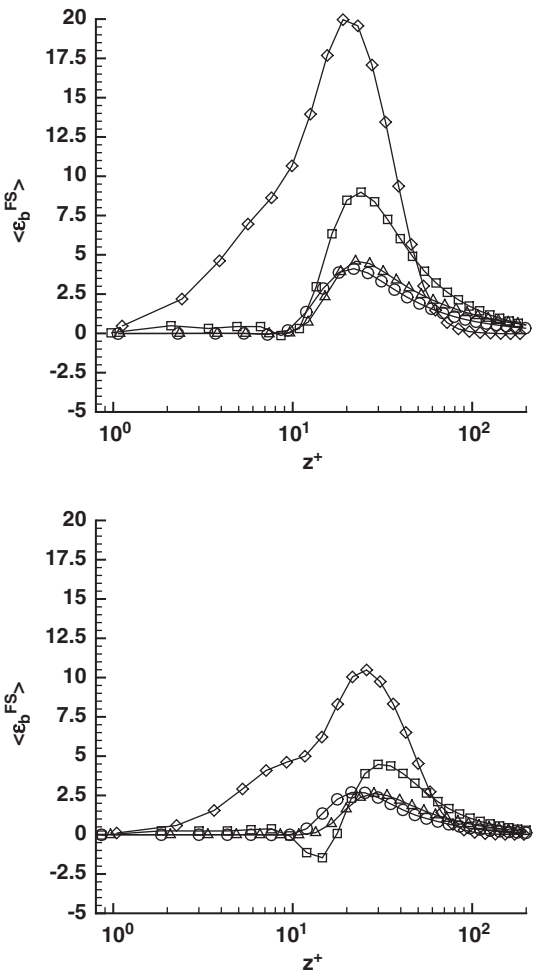

Figure 14. Fluctuating strain SGS dissipation $\langle \varepsilon_{FS} \rangle$ profile normalized by the bulk velocity, the molecular viscosity and the channel height on the fine (top) and coarse (bottom) grid. Caption: see Figure 1.

Scale model. The occurence of these negative values were predicted by previous DNS *a priori* tests, and corresponds to the backscatter phenomena. A very carefull analysis of the figures reveals that all the selective models (on the two grids) exhibit negative values (but with very small amplitudes) in the $z^+ \approx 10$ region. As already observed by Härtel and Kleiser [4], the Germano–Lilly dynamic model predicts a strictly positive fluctuating strain dissipation, and is then not capable to account in a proper way for the backscatter.

It is also remarked that, as the grid is refined, the negative values tend to disappear, in agreement with the DNS analysis. This is due to the fact that, on the fine grid, the turbulent coherent events which are responsible for the backward energy transfer are captured in a quasi-direct manner by the simulation, and do not require parametrization.

The capability of strictly positive subgrid viscosity SGS models to account for the backscatter effect is now investigated by operating a new decomposition of the fluctuating strain dissipation term. When a subgrid viscosity model is employed, the parametrized subgrid tensor appears as the product of the subgrid viscosity and the resolved deformation tensor. By splitting these two terms as the sum of a mean and a fluctuating part, and inserting into Equation (39), one obtains the following triple decomposition for $\langle \varepsilon_{\mathrm{FS}} \rangle$:

$$\begin{aligned} \langle \varepsilon_{\mathrm{FS}} \rangle &= -\langle \tau''_{ij} \bar{S}''_{ij} \rangle \\ &= \langle \nu''_{\mathrm{sgs}} \bar{S}''_{ij} \rangle \langle \bar{S}_{ij} \rangle + \langle \nu_{\mathrm{sgs}} \rangle \langle \bar{S}''_{ij} \bar{S}''_{ij} \rangle + \langle \nu''_{\mathrm{sgs}} \bar{S}''_{ij} \bar{S}''_{ij} \rangle \end{aligned} \tag{40}$$

The first term on the right-hand side corresponds to the transfer of energy due to the interaction of the fluctuations of the subgrid tensor and the mean strain, the second one to the transfer induced by the correlation between the mean subgrid viscosity and the fluctuating velocity gradient, and the third term represents the transfer associated to the fluctuations of the SGS tensor and the fluctuating velocity field. It can be noticed that only the second term is identified as a strictly positive quantity, while the other two can have negative values. Mean profiles of these three terms, respectively, referred to as $\varepsilon_{\mathrm{FS1}}$, $\varepsilon_{\mathrm{FS2}}$ and $\varepsilon_{\mathrm{FS3}}$ are presented in Figures 15–17.

An important difference between the Germano–Lilly dynamic procedure and the use of the selection function is identified: selective models yield negative values for both $\varepsilon_{\mathrm{FS1}}$ and $\varepsilon_{\mathrm{FS3}}$, while the dynamic model predicts only strictly positive values for $\varepsilon_{\mathrm{FS1}}$. Taking into account the fact that only the components $\langle \bar{S}_{13} \rangle$ and $\langle \bar{S}_{31} \rangle$ of the mean resolved stress tensor are non-zero, the term $\langle \varepsilon_{\mathrm{FS1}} \rangle$ reduces to:

$$\langle \varepsilon_{\mathrm{FS1}} \rangle = -2 \langle \nu''_{\mathrm{sgs}} \bar{S}''_{13} \rangle \langle \bar{S}_{13} \rangle \tag{41}$$

This relationship shows that the origin of the reverse energy cascade is the existence of a negative correlation of the fluctuating part of the wall-normal parametrized subgrid stress and the wall-normal derivative of the streamwise grid-scale velocity component. The *a priori tests* of Härtel and Kleiser [4] have shown that this mechanism is the one which is effectively responsible for the main part of the backscatter. The fact that negative values of $\varepsilon_{\mathrm{FS1}}$ are observed for the two grids and the three models demonstrates that the capability of predicting backscatter is an intrisic property of the selection function. That function provides a conditional application of the SGS model, in a coherent way with the observation of Piomelli *et al.* [3] that the kinetic energy transfers are associated with intermittent coherent turbulent events. This can prevent the spurious coupling between the resolved velocity gradient and the kinetic energy transfer which is induced by the classical subgrid viscosity models, and then permits the capture of the backscatter by allowing the existence of a phase shift between the mean shear and the wall-normal subgrid stress.

As previously shown in Härtel and Kleiser [4] the dynamic model is unable to avoid that spurious coupling, and does not recover the backscatter in a physical way. But the location of the negative peak of $\varepsilon_{\mathrm{FS3}}$ seems to indicate that the dynamic procedure, by modifying the value of Smagorinsky constant c_1, is sensitive to the existence of a backscatter process in the buffer region.

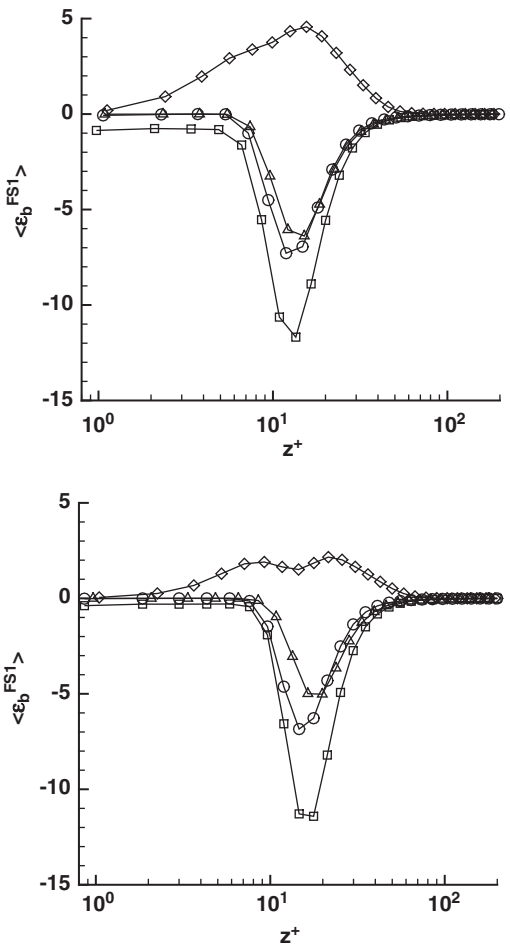

Figure 15. $\langle \varepsilon_{FS1} \rangle$ profile normalized by the bulk velocity, the molecular viscosity and the channel height on the fine (top) and coarse (bottom) grid. Caption: see Figure 1.

7. CONCLUSIONS

New self-adaptive SGS models have been proposed on the basis of subgrid viscosity models (Smagorinsky model and Mixed Scale model) and the continuous selective function. The SGS models have been written in a fully general way, which do not incorporate any information dealing with the topology of the flow, and have been discretized using narrow compact-stencil discrete operators. In order to assess the capability of the resulting self-adaptive models to yield reliable results for future industrial applications in complex geometries, simulations of a plane channel flow on two grids have been carried out with a second-order accurate numerical method.

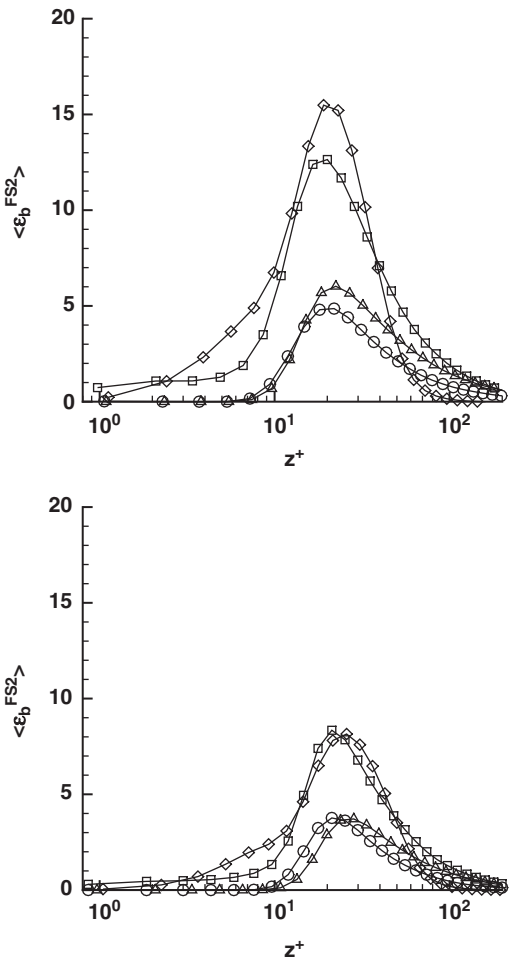

Figure 16. $\langle \varepsilon_{FS2} \rangle$ profile normalized by the bulk velocity, the molecular viscosity and the channel height on the fine (top) and coarse (bottom) grid. Caption: see Figure 1.

That approach was found to be efficient, in the sense that the modified models are able to capture the transition process and do not lead to relaminarization, while the basic version of the Smagorinsky and Structure Function models do not have these properties. The proposed selective SGS models give satisfactory results, whose quality is at least as good as those of the dynamic Smagorinsky model. Another advantage of the selective models is that they are well-defined and do not necessitate the use of a stabilization technique, as the dynamic model does.

A very interesting fact is that the use of the selection function enables the representation of the backscatter due to the fluctuating strain dissipation in the buffer layer, while dynamic model does not. The new proposed triple decomposition of that quantity reveals that this

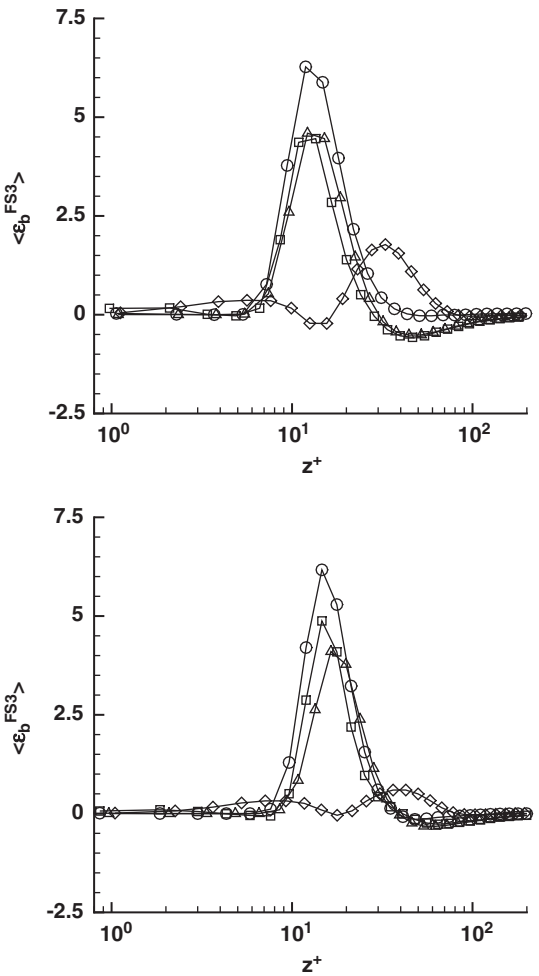

Figure 17. $\langle \varepsilon_{FS3} \rangle$ profile normalized by the bulk velocity, the molecular viscosity and the channel height on the fine (top) and coarse (bottom) grid. Caption: see Figure 1.

capability is due to the conditional use of the subgrid viscosity introduced by the selection function, which can to recover a physical correlation between the mean shear and the subgrid tensor fluctuations.

REFERENCES

1. Sagaut P. *Large-Eddy Simulations for Incompressible Flows*: *an Introduction*. Springer: Berlin, 2001.
2. Härtel C, Kleiser L, Unger F, Friedrich R. Subgrid-scale energy transfer in the near-wall region of turbulent flows. *Physics of Fluids* 1994; **6**(9):3130–3143.
3. Piomelli U, Yu Y, Adrian RJ. Subgrid-scale energy transfer and near-wall turbulence structure. *Physics of Fluids* 1996; **8**(1):215–224.
4. Härtel C, Kleiser L. Analysis and modelling of subgrid-scale motions in near-wall turbulence. *Journal of Fluid Mechanics* 1998; **356**:327–352.

5. Mary I, Sagaut P. LES of a flow around an airfoil near stall. *AIAA Journal* 2002; **36**:1139–1145.
6. Piomelli U, Moin P, Ferziger JH. Model consistency in large eddy simulation of turbulent channel flows. *Physics of Fluids* 1988; **31**(7):1884–1891.
7. Schumann U. Subgrid scale model for finite difference simulations of turbulent flows in plane channels and annuli. *Journal of Computational Physics* 1975; **18**:376–404.
8. David E. *Modélisation des écoulements compressibles et hypersoniques: une approche instationnaire*. Thèse de Doctorat, Institut National Polytechnique de Grenoble, 1993.
9. Métais O, Lesieur M. Spectral large-eddy simulation of isotropic and stably stratified turbulence. *Journal of Fluid Mechanics* 1992; **239**:157–194.
10. Sagaut P, Troff B. Subgrid-scale model improvements for non-homogeneous flows. In *Advances in DNS/LES*, Liu C, Liu Z (eds), Greyden Press, 1997; 401–408.
11. Kim J, Moin P, Moser R. Turbulence statistics in fully developed channel flow at low Reynolds number. *Journal of Fluid Mechanics* 1987; **177**:133–166.
12. Mansour N, Moser R, Kim J. PCH11: Fully developed turbulent channel flow simulations. *A selection of test cases for the validation of Large-Eddy Simulations of turbulent flows—AGARD Advisory Report 345*, NATO, 1998.
13. Smagorinsky J. General circulation experiments with the primitive equations. *Monthly Weather Review* 1963; **91**:99–164.
14. Deardorff JW. A numerical study of three-dimensional turbulent channel flow at large Reynolds number. *Journal of Fluid Mechanics* 1970; **41**:453–480.
15. Sagaut P. Numerical simulations of separated flows with subgrid models. *Recherche Aérospatiale* (*english version*) 1996; **1**:51–63.
16. Germano M, Piomelli U, Moin P, Cabot WH. A dynamic subgrid-scale eddy viscosity model. *Physics of Fluids A* 1991; **3**(7):1760–1765.
17. Lilly DK. A proposed modification of the Germano subgrid-scale closure method. *Physics of Fluids A* 1992; **4**(3):633–635.
18. Lesieur M, Métais O. New trends in large-eddy simulations of turbulence. *Annual Review of Fluid Mechanics* 1996; **28**:45–82.
19. Lê TH, Troff B, Sagaut P, Dang-Tran K, Loc TP. PEGASE: a Navier–Stokes solver for direct numerical simulation of incompressible flows. *International Journal for Numerical Methods in Fluids* 1997; **24**:833–861.
20. Kravenchko AG, Moin P. On the effect of numerical errors in large-eddy simulations of turbulent flows. *Journal of Computational Physics* 1997; **131**:310–322.
21. van der Vorst E. Bi-CGSTAB: a fast and smoothly converging variant of Bi-CG for the solution of nonsymetric linear systems. *Journal of Scientific Computing* 1992; **13**:631–644.
22. Strikwerda JC. Finite difference methods for the Stokes and Navier-Stokes equations, *SIAM Journal on Scientific and Statistical Computing* 1984; **5**(1):56.
23. Deschamps V. Simulation numérique de la turbulence inhomogène incompressible dans un écoulement de canal plan. *Technical Report*, ONERA, 1988.
24. Comte P, Lee S, Cabot W. A subgrid-scale model based on the second-order velocity structure function. *Annual Research Briefs*, *Center for Turbulence Research* 1990; 31–46.
25. Najjar FM, Tafti DK. Study of discrete test filters and finite difference approximations for the dynamic subgrid-scale stress model. *Physics of Fluids* 1996; **8**(4):1076–1088.
26. Gresho P. Incompressible Fluid Dynamics: some fundamental formulation issues. *Annual Review of Fluid Mechanics* 1991; **23**:413–453.
27. Winckelmans G, Jeanmart H, Carati D. On the comparison of turbulence intensities from large-eddy simulation with those from experiment or direct numerical simulation. *Physics of Fluids* 2002; **14**(5):1809–1811.
28. Zahrai S, Bark FH, Karlsson RI. On anisotropic subgrid modelling. *European Journal of Mechanics B/Fluids* 1995; **14**(4):459–486.
29. Sarghini F, Piomelli U, Balaras E. Scale-similar models for large-eddy simulations. *Physics of Fluids* 1999; **11**(6):1596–1607.
30. Zang T. Numerical simulation of the dynamics of turbulent boundary layers: perspectives of a transition simulator. *Philosophical Transaction of The Royal Society of London A* 1991; **336**:95–102.
31. Antonia RA, Teitel M, Kim J, Browne LWB. Low-Reynolds-number effect in a fully developed turbulent channel flow. *Journal of Fluid Mechanics* 1992; **236**:579–605.
32. Cabot W. Local dynamic subgrid-scale models in channel flow. *Annual Research Briefs, Center for Turbulence Research* 1994, 143–159.
33. Lamballais E, Métais O, Lesieur M. Spectral dynamic model for large-eddy simulations of turbulent rotating channel flow. *Theoretical and Computational Fluid Dynamics* 1998; **12**:149–177.
34. Piomelli U. High Reynolds number calculations using the dynamic subgrid-scale stress model. *Physics of Fluids A* 1993; **5**(6):1484–1490.

